Control of flow around a circular cylinder for minimizing energy dissipation

Hiroshi Naito and Koji Fukagata

Department of Mechanical Engineering, Keio University, Hiyoshi 3-14-1, Kohoku-ku, Yokohama 223-8522, Japan

(Received 11 December 2013; revised manuscript received 22 August 2014; published 17 November 2014; corrected 18 December 2014)

Control of flow around a circular cylinder is studied numerically aiming at minimization of the energy dissipation. First, we derive a mathematical relationship (i.e., identity) between the energy dissipation in an infinitely large volume and the surface quantities, so that the cost function can be expressed by the surface quantities only. Subsequently a control law to minimize the energy dissipation is derived by using the suboptimal control procedure [J. Fluid Mech. **401**, 123 (1999)]. The performance of the present suboptimal control law is evaluated by a parametric study by varying the value of the arbitrary parameter contained. Two Reynolds numbers, Re = 100 and 1000, are investigated by two-dimensional simulations. Although no improvement is obtained at Re = 100, the present suboptimal control shows better results at Re = 1000 than the suboptimal controls previously proposed. With the present suboptimal control, the dissipation and the drag are reduced by 58% and 44% as compared to the uncontrolled case, respectively. The suction around the front stagnation point and the blowing in the rear half are found to be weakened as compared to those in the previous suboptimal control targeting at pressure drag reduction. A predetermined control based on the control input profile obtained by the suboptimal control is also performed. The energy dissipation and the drag are found to be reduced as much as those in the present suboptimal control. It is also found that the present suboptimal and predetermined controls have better energy efficiencies than the suboptimal control previously proposed. Investigation at different control amplitudes reveals an advantage of the present control at higher amplitude. Toward its practical implementation, a localized version of the predetermined control is also examined, and it is found to work as effectively as the continuous case. Finally, the present predetermined control is confirmed to work well in a three-dimensional flow too.

DOI: 10.1103/PhysRevE.90.053008 PACS number(s): 47.85.L−

I. INTRODUCTION

Recent progress in numerical simulations, microelectromechanical systems technologies, and control theories have led to growing interests in flow control [1–4]. The most notable example is the control of flow around a bluff body [5]. It could contribute not only to a drag reduction but also to a suppression of flow oscillations, both leading to mitigation of environmental impacts.

Among the recent studies, the suboptimal control for a flow around a circular cylinder by Min and Choi [6] is of great importance in the sense that a practical control law can be derived on a solid theoretical basis. Although the optimal control, which attempts to minimize or maximize a cost function in a relatively long time horizon, is theoretically more rigorous, it usually requires an extremely high computational cost for iteratively solving the forward and the adjoint equations [7]. In contrast, the suboptimal control attempts to minimize or maximize a cost function in a relatively short time horizon, by which the iterative computations are avoided.

For an active control to be practical, the total power, i.e., the summation of the propulsive (or pumping) power and the actuation power, should be less than the propulsive (or pumping) power of the uncontrolled case. The total power is identical to the energy dissipation rate at the statistically steady state. For drag reduction of a flow in a straight or a constant-curvature duct, it has mathematically been proved [8] the lowest total power is achieved when the flow takes the Stokes flow profile. Although such a lower bound has not been proved for an external flow, such as a flow around a circular cylinder, it is still common that the energy dissipation rate should be the most proper quantity to be reduced by an active control. Intuitively speaking, the ultimate state may be a state with no energy dissipation, where all the strain vanishes, leading to no frictional or pressure drag; in such a state the unsteadiness of flow and the associated aerodynamic noise will also vanish.

In the present study, we attempt to reduce the energy dissipation in the flow around a circular cylinder. Since the energy dissipation rate is a quantity defined as a volume integral, it cannot be directly measured by sensors placed on the cylinder surface; namely, the energy dissipation rate itself cannot be used as the cost function to be minimized. Therefore, we first derive the mathematical relationship (i.e., identity) between the energy dissipation in an infinitely large volume and the surface quantities, so that the cost function can be expressed by the surface quantities only. Using the identity derived, we derive the control law minimizing the cost function following the suboptimal control procedure in Ref. [6]. The performance of the present suboptimal control is evaluated by two-dimensional numerical simulations of flows around a circular cylinder. Toward its practical implementation, we also examine the performance of a predetermined (i.e., open-loop) control using the control input profile obtained by the suboptimal control and its localized version. Finally, effectiveness of the present predetermined control is assessed in a three-dimensional flow.

II. IDENTITY BETWEEN THE ENERGY DISSIPATION IN AN INFINITE VOLUME AND THE SURFACE QUANTITIES

In this section, we first derive the mathematical relationship between the energy dissipation in an infinitely large volume and the surface quantities.

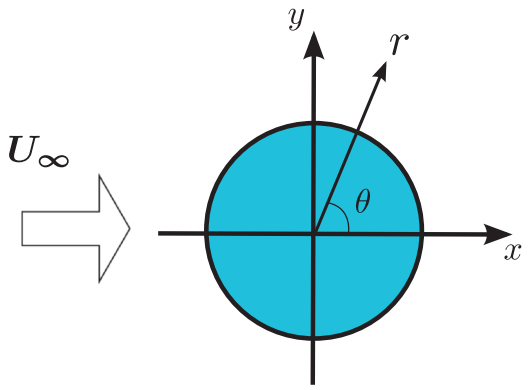

FIG. 1. (Color online) Flow around a circular cylinder.

We consider a uniform flow around a fixed circular cylinder of radius R, as shown in Fig. 1. The governing equations are the incompressible Navier-Stokes equation,

$$\frac{\partial \mathbf{u}}{\partial t} = -\nabla \cdot \left[\mathbf{u}\mathbf{u} + p\mathbf{I} - \frac{2}{\mathrm{Re}}\mathbf{s} \right], \tag{1}$$

and the continuity equation,

$$\nabla \cdot \mathbf{u} = 0, \tag{2}$$

where $\mathbf{u}$ and p denote the velocity vectors and the pressure, respectively; $\mathbf{I}$ and $\mathbf{s}$ are the unit dyadic and the strain-rate tensor,

$$\mathbf{s} = \tfrac{1}{2}[\nabla \mathbf{u} + (\nabla \mathbf{u})^T]. \tag{3}$$

All quantities are made dimensionless by the fluid density ρ, the cylinder diameter, D, and the free-stream velocity, U_∞; the Reynolds number is defined as $\mathrm{Re} = U_\infty D/\nu$, where ν denote the kinematic viscosity.

To derive the mathematical relationship, we consider a control volume as shown in Fig. 2. The cylinder is at rest in a uniform velocity of $\mathbf{U}_\infty = U_\infty \mathbf{e}_x$. We assume that the flow is controlled by a zero-net-flux blowing and suction continuously distributed over the surface; the surface velocity is $\mathbf{u}_s(\theta) = \phi(\theta)\mathbf{n}$. We also assume that the outer boundary, ∂V_2, is located infinitely far from the cylinder surface, ∂V_1.

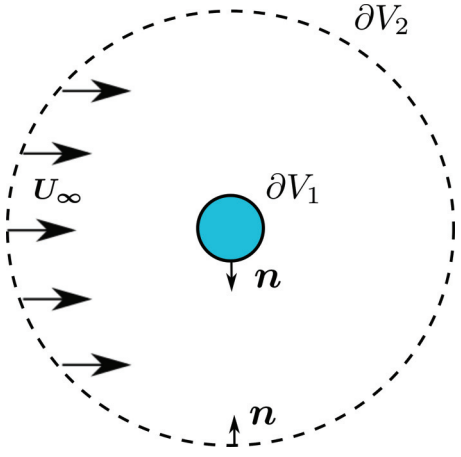

FIG. 2. (Color online) Control volume.

The key technique used to derive the cost function is to introduce the deviation from the uniform velocity:

$$\mathbf{u}' = \mathbf{u} - U_\infty \mathbf{e}_x. \tag{4}$$

Then the velocity deviation on ∂V_2 is zero and that on ∂V_1 is expressed as

$$\mathbf{u}'_s = \mathbf{u}_s - U_\infty \mathbf{e}_x = \phi \mathbf{n} - U_\infty \mathbf{e}_x. \tag{5}$$

By this, the present problem becomes similar to the classical problem considering the drag exerting on a circular cylinder moving in a quiescent fluid [9]. Note that the strain-rate tensor based on the velocity deviation is identical to that based on the velocity itself, $\mathbf{s}' = \mathbf{s}$.

The equation for the energy balance based on $\mathbf{u}'$ is derived by taking an inner product between $\mathbf{u}'$ and Eq. (1) expressed by $\mathbf{u}'$:

$$\frac{\partial \left(\frac{1}{2}\mathbf{u}' \cdot \mathbf{u}'\right)}{\partial t} = -\nabla \cdot \left[\frac{1}{2}(\mathbf{u}' \cdot \mathbf{u}')(\mathbf{u}' + U_\infty \mathbf{e}_x) + p\mathbf{u}' \right] + \frac{2}{\mathrm{Re}} \mathbf{u}' \cdot \nabla \cdot \mathbf{s}'. \tag{6}$$

The global energy balance is obtained by integrating Eq. (6) in the volume. By using Gauss's divergence theorem and by noting $\mathbf{u}' = 0$ on ∂V_2, the integration of the first term in the right-hand-side becomes

$$-\int_V \nabla \cdot \left[\frac{1}{2}(\mathbf{u}' \cdot \mathbf{u}')(\mathbf{u}' + U_\infty \mathbf{e}_x) + p\mathbf{u}' \right] dv = \int_{\partial V_1} \left[\frac{1}{2}(\phi^3 - 2\phi^2 U_\infty \cos\theta) + (p\phi - pU_\infty \cos\theta) \right] ds. \tag{7}$$

By using some vector identities, the integration in the second term yields [8]

$$\begin{aligned} &\int_V \mathbf{u}' \cdot \nabla \cdot \mathbf{s}' dv \\ &= -\int_V \mathbf{s}' : \mathbf{s}' dv - \int_{\partial V_1} \mathbf{n} \cdot \mathbf{s}' \cdot \mathbf{u}' \, ds \\ &= -\int_V \mathbf{s}' : \mathbf{s}' dv - \int_{\partial V_1} \mathbf{n} \cdot \mathbf{s}' \cdot (\phi \mathbf{n} - U_\infty \mathbf{e}_x) \, ds \\ &= -\int_V \mathbf{s} : \mathbf{s} dv + \int_{\partial V_1} \left(\frac{1}{R}\phi^2 \right) ds + U_\infty \int_{\partial V_1} \mathbf{n} \cdot \mathbf{s} \cdot \mathbf{e}_x \, ds. \end{aligned} \tag{8}$$

By rearranging the equations above, the global energy balance is finally expressed as

$$\varepsilon = -\int_V \frac{\partial \left(\frac{1}{2}\mathbf{u}' \cdot \mathbf{u}'\right)}{\partial t} dv + U_\infty (F_{DP} + F_{DF} + F_{D\phi}) + W_{id}, \tag{9}$$

where the dissipation rate, ε, the pressure drag, F_{DP}, the friction drag, F_{DF}, and the additional drag due to the blowing and suction, $F_{D\phi}$, can be derived by taking an inner product of

$\mathbf{e}_x$ and a volume integration of Eq. (1), as

$$\varepsilon = \frac{2}{\mathrm{Re}} \int_V \mathbf{s} : \mathbf{s}\, dv, \tag{10}$$

$$F_{DP} = \int_{\partial V_1} (-p \cos\theta)\, ds, \tag{11}$$

$$F_{DF} = \frac{2}{\mathrm{Re}} \int_{\partial V_1} \mathbf{n} \cdot \mathbf{s} \cdot \mathbf{e}_x\, ds, \tag{12}$$

and

$$F_{D\phi} = \int_{\partial V_1} (-\phi^2 \cos\theta)\, ds, \tag{13}$$

respectively, and the ideal actuation power, W_{id}, is computed as

$$W_{id} = \int_{\partial V_1} \left[\left(p + \frac{1}{2}\phi^2 \right) \phi + \frac{2}{\mathrm{Re}} \frac{1}{R} \phi^2 \right] ds. \tag{14}$$

The first term (i.e., the time derivative term) in Eq. (9) is exactly zero for a steady flow; it may also be neglected in general if we take a reasonable time average, such as an average in one period of vortex shedding. Hence, the energy dissipation at the statistically steady (or quasisteady) state, the reasonably time-averaged dissipation rate, $\overline{\varepsilon}$, is finally expressed by using the quantities on the surface only, as

$$\overline{\varepsilon} = U_\infty \left(F_{DP} + F_{DF} + F_{D_\phi} \right) + W_{id}. \tag{15}$$

III. A SUBOPTIMAL CONTROL LAW

To minimize the energy dissipation expressed above using the surface quantities, we derive a control law by following the suboptimal control procedure of Min and Choi [6].

Since this suboptimal control theory [6] utilizes the linearization of the governing equations through their temporal discretization, the control input depends on how they are temporally discretized. In the present study, we apply an explicit method for the nonlinear term and an implicit method for the linear terms, which gives a temporally discretized form:

$$\mathbf{u}^{n+1} + \Delta t_c \nabla p^{n+1} - \frac{\Delta t_c}{\mathrm{Re}} \nabla^2 \mathbf{u}^{n+1} = \mathbf{F}^n, \tag{16}$$

$$\nabla \cdot \mathbf{u}^{n+1} = 0, \tag{17}$$

where $\mathbf{F}^n$ is the explicit part of the Navier-Stokes equation and the superscripts n and $n+1$ denote the present and next time steps, respectively; Δt_c denotes the time width of control, which is an arbitrary parameter chosen independently of the simulation time step. The boundary conditions are given as

$$\begin{aligned} u_r(R,\theta) &= \phi(\theta), \quad \lim_{r\to\infty} u_r(r,\theta) = U_\infty \cos\theta, \\ u_\theta(R,\theta) &= 0, \quad \lim_{r\to\infty} u_\theta(r,\theta) = -U_\infty \sin\theta. \end{aligned} \tag{18}$$

The original suboptimal control proposed by Choi *et al.* [10] is based on the gradient descent method. At each time instant, a cost function J can be reduced by an iterative algorithm given by

$$\phi^{l+1} - \phi^l = -\rho \frac{\mathscr{D} J(\phi^l)}{\mathscr{D}\phi}, \tag{19}$$

where

$$\frac{\mathscr{D} J}{\mathscr{D}\phi^l} \tilde{\phi} = \lim_{h\to 0} \frac{J(\phi^l + h\tilde{\phi}) - J(\phi^l)}{h} \tag{20}$$

is the Fréchet differential with $\tilde{\phi}(\theta)$ being a perturbation to the control input $\phi(\theta)$; the superscript l denotes the iteration index, and the parameter ρ is a positive number. However, those authors [10] concluded from their numerical test that a single iteration is sufficient in the case of suboptimal control. Namely, the control input is simply obtained by a single iteration starting from the initial value of $\phi^0 = 0$, which reads

$$\phi = -\rho \frac{\mathscr{D} J(\phi)}{\mathscr{D}\phi}. \tag{21}$$

For the present cost function, i.e., $J = \overline{\varepsilon}$ (Eq. (15)), the gradient $\mathscr{D}J/\mathscr{D}\phi$ can be computed as

$$\begin{aligned} \frac{\mathscr{D} J}{\mathscr{D}\phi} = \frac{1}{2\pi} \int_0^{2\pi} \Bigg[& U_\infty \{ \underbrace{-\Pi(r,\tau-\theta)\cos\tau}_{\text{pressure drag}} \} \\ & + U_\infty \underbrace{\frac{1}{\mathrm{Re}} \frac{\partial}{\partial r} (\eta_r(r,\tau-\theta)\cos\tau - \eta_\theta(r,\tau-\theta)\sin\tau)}_{\text{friction drag}} \\ & + \underbrace{\{u_r \Pi(r,\tau-\theta) + p\eta_r(r,\tau-\theta)\} + \frac{3}{2} {u_r}^2 \eta_r(r,\tau-\theta)}_{\text{actuation power}} \\ & - \underbrace{\frac{4}{\mathrm{Re}} \frac{1}{R} u_r \eta_r(r,\tau-\theta)}_{\text{actuation power}} - \underbrace{2 u_r \eta_r(r,\tau-\theta) U_\infty \cos\tau}_{\text{additional drag}} \Bigg]_{r=R} d\tau. \end{aligned} \tag{22}$$

Here the label under each term corresponds to the gradient of each term in the cost function (15). The functions, $\eta_r(r,\tau)$, $\eta_\theta(r,\tau)$, and $\Pi(r,\tau)$, are the impulse responses given by the solution to the following set of equations [11]:

$$\eta + \Delta t_c \nabla \Pi - \frac{\Delta t_c}{\mathrm{Re}} \nabla^2 \eta = 0, \tag{23}$$

$$\nabla \cdot \eta = 0, \tag{24}$$

with the boundary conditions

$$\begin{aligned} \eta_r(R,\theta) &= \delta(\theta), \quad \lim_{r\to\infty} \eta_r(r,\theta) = 0, \\ \eta_\theta(R,\theta) &= 0, \quad \lim_{r\to\infty} \eta_\theta(r,\theta) = 0, \end{aligned} \tag{25}$$

where $\delta(\theta)$ denotes the Dirac delta function. The solutions are expressed in the Fourier space as

$$\hat{\Pi}_{k=0} = \hat{\Pi}_{r=R} = \text{const}, \tag{26}$$

$$\hat{\Pi}_{k\neq 0} = \frac{1}{\Delta t_c} \frac{1}{|k|} \frac{A}{B} \left(\frac{R}{r} \right)^{|k|}, \tag{27}$$

$$\hat{\eta}_{r,k=0} = \frac{K_1(mr)}{K_1(mR)}, \tag{28}$$

$$\hat{\eta}_{r,k\neq 0} = \frac{A\,(R/r)^{|k|} + R|k|K_{|k|}(mr)}{Br}, \tag{29}$$

$$\hat{\eta}_{\theta,k=0} = 0, \tag{30}$$

and

$$\hat{\eta}_{\theta,k\neq 0} = \frac{i|k|}{k}\frac{-A(R/r)^{|k|} + \{R|k|K_{|k|}(mr) - mRrK_{|k|+1}(mr)\}}{Br}, \tag{31}$$

where

$$A = R|k|K_{|k|}(mR) - mR^2K_{|k|+1}(mR), \tag{32}$$

$$B = 2|k|K_{|k|}(mR) - mRK_{|k|+1}(mR), \tag{33}$$

and

$$m = \sqrt{\frac{\mathrm{Re}}{\Delta t_c}}. \tag{34}$$

Here k denotes the wave number in the circumferential direction and $K_{|k|}(r)$ is the $|k|$th order modified Bessel function of the second kind.

As is clear from the expressions above, the control input depends on the arbitrary control interval, Δt_c, which should be optimized to obtain the best result. We will discuss this point in Sec. V.

IV. NUMERICAL PROCEDURE

For the present numerical simulations, the direct numerical simulation code of Naito and Fukagata [12] is used. For the spatial discretization, the second-order energy-conservative finite difference method in the cylindrical coordinate system [13] is used; for the temporal integration, the low-storage third order Runge-Kutta/Crank-Nicolson scheme [14] is applied with the higher-order fractional-step method [15] for the velocity-pressure coupling. The pressure Poisson equation is solved by using the fast Fourier transform in the circumferential direction and the tridiagonal matrix algorithm in the radial direction.

The radius of the computational domain is set to be 70 times of the cylinder radius, R. A uniform velocity, U_∞, is imposed at the inlet boundary ($0 \leqslant |\theta| \leqslant \frac{3}{4}\pi$) and the convective boundary condition is adopted at the outlet boundary ($\frac{3}{4}\pi \leqslant |\theta| \leqslant \pi$). The number of computational points is $N_r \times N_\theta = 220 \times 256$ in r and θ directions, respectively.

The present numerical code and the computational conditions for the base flow (i.e., the uncontrolled flow) have been verified and validated through an extensive comparison with the literature [12].

In the numerical implementation of control input, actuators and sensors of infinitesimal dimensions are assumed to be continuously distributed over the entire cylinder surface. We also apply a temporal filter (i.e., an exponentially weighted moving average) to the control input to avoid numerical instabilities, as $\phi^n = (7/10)\phi^F + (3/10)\phi^{n-1}$, where n is the simulation time step and ϕ^F is the input obtained in Eq. (21).

V. RESULTS AND DISCUSSION

A. Suboptimal control

Performance of the present suboptimal control is assessed by numerical simulations. For comparison, we also perform simulations using the suboptimal control of Ref. [6], which is based on the cost functions J_1 and J_2. The first cost function, J_1, aims at minimization of the pressure drag,

$$J_1 = \int_{\partial V_1} (-p\cos\theta)\,ds. \tag{35}$$

It gives an analytical solution for the control input,

$$\phi(\theta) = -\phi_{\max}\cos\theta, \tag{36}$$

where $\phi_{\max}$ denotes the amplitude. The second cost function, J_2, aims at minimization of the difference between the actual pressure distribution, p, and the target (i.e., inviscid) pressure distribution, p_t,

$$J_2 = \frac{1}{2}\int_{\partial V_1} (p_t - p)^2\,ds. \tag{37}$$

In term of the drag (but not the total power or the dissipation), Min and Choi [6] report that J_2 gives the best result. Hereafter, these controls are referred to as the J_1 control and J_2 control, respectively.

In all cases, the coefficient ρ in Eq. (21) is determined so as to have a given maximum amplitude, $\phi_{\max}$. In this study, we fix it to $\phi_{\max} = 0.4$, where a complete suppression of vortex shedding at $\mathrm{Re} = 100$ has been achieved previously [6]. The Reynolds numbers are $\mathrm{Re} = 100$ and $\mathrm{Re} = 1000$. Although the actual flow at $\mathrm{Re} = 1000$ should have three-dimensionality, we first perform two-dimensional simulations to compare the control performance with $\mathrm{Re} = 100$ cases.

As noted in Sec. III, the control input depends on the arbitrary parameter, Δt_c. Therefore, first, we perform a parametric study to determine the optimal value of Δt_c. The dissipation rate is computed using Eq. (15) after the flow reaches its statistically steady state. For the computational domain of a finite size, a summation of the dissipation directly computed inside the computational domain, i.e., $(2/\mathrm{Re})\int_V (\mathbf{s}:\mathbf{s})\,dv$, and the energy flowing out from the outflow boundary should balance $\overline{\varepsilon}$ in Eq. (15). For the cases presented below, the error in this balance has been verified to be sufficiently small.

The dissipation rate, $\overline{\varepsilon}$, computed for different values of $\Delta t_c/T$ at $\mathrm{Re} = 100$ and $\mathrm{Re} = 1000$ are shown in Fig. 3. In all cases the dissipation is found to be reduced as compared to the uncontrolled case. When $\Delta t_c/T$ is small, $\overline{\varepsilon}$ in the present suboptimal control takes a similar value to that of the J_1 control, e.g., $\overline{\varepsilon} = 0.378$ at $\mathrm{Re} = 1000$. This is because the first term in Eq. (22) is dominant at $\Delta t_c/T \ll 1$; namely, the cost function becomes similar to that minimizing the pressure drag [Eq. (35)].

At $\mathrm{Re} = 100$, the dissipation in the present control takes similar values at a different value of $\Delta t_c/T$, and it is slightly increased for longer control time steps. The statistics (not shown) suggest that the actuation power is increased with the increase of $\Delta t_c/T$, while the drag and the flow pattern are nearly unchanged. Reference [6] reports that J_2 control gives the best result in terms of drag reduction at $\mathrm{Re} = 100$. In the present simulations as well, the drag was found to be

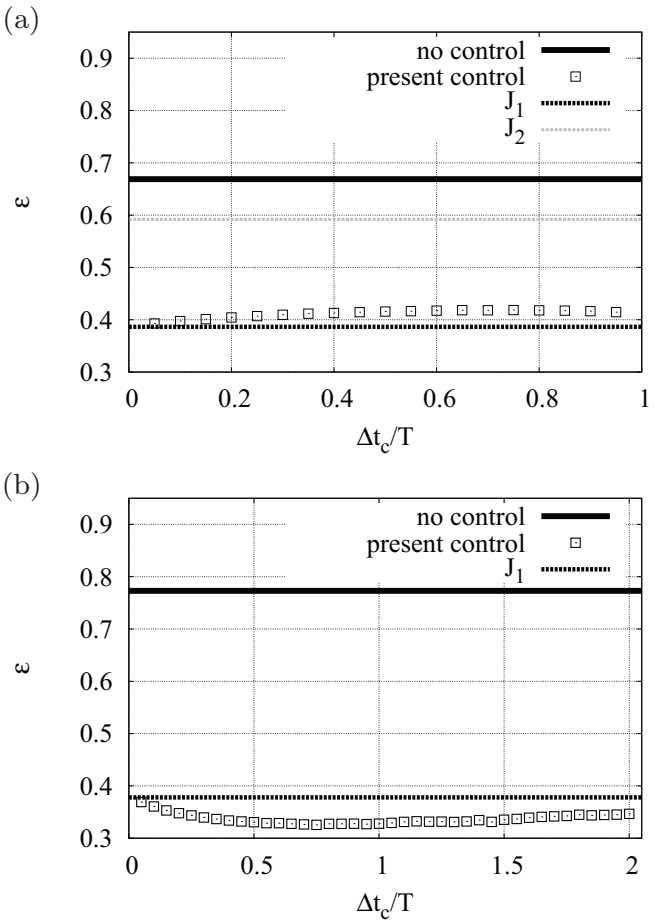

FIG. 3. Parametric study: (a) Re = 100; (b) Re = 1000. The dissipation rate ε is made dimensionless by ρ, U_∞, and D.

the smallest in the J_2-control case. However, the dissipation turned out to be much larger than those of the J_1 control and the present suboptimal control due to a greater actuation power required to enforce the pressure distribution to fit the target.

In the present simulation with J_2 control at Re = 1000, the error in the energy balance noted above was found to be non-negligibly small due to numerical instabilities likely inherent to the control law [hence not shown in Fig. 3(b)]. In principle, however, the J_2 control is expected to have a higher energy dissipation rate than the J_1 control due to its higher actuation power required, as observed at Re = 100. In the case with the present control at Re = 1000, dissipation is reduced as the increase of $\Delta t_c/T$. The minimum value obtained at $\Delta t_c/T = 0.75$ corresponds to 13.2% reduction compared to that in the J_1 control. In the followings, we discuss some details in the case of $\Delta t_c/T = 0.75$ at Re = 1000, where the control effect is maximized.

Figure 4 shows the profile of control input, $\phi(\theta')$, i.e., the radial velocity on the cylinder surface, $u_r|_{r=R}$, where $\theta' = 180^\circ - \theta$ denotes the angle from the front stagnation point. Although the velocity distribution in the present suboptimal control case is basically similar to that in the J_1-control case, the suction near the front stagnation point, $\theta' = 0^\circ$, and the blowing in the rear half, $\theta' = 180^\circ$, are observed to have been weakened in different manners.

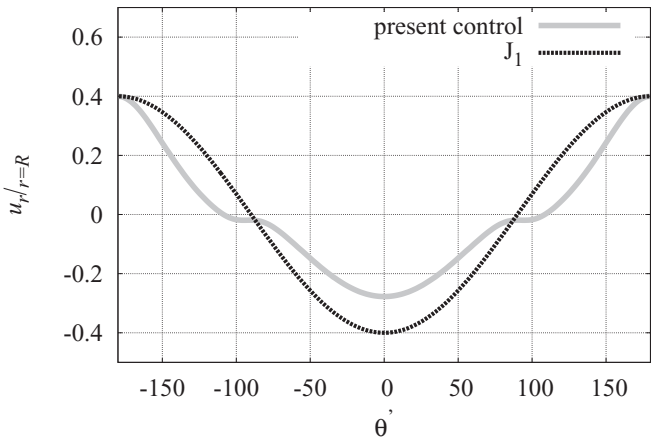

FIG. 4. Velocity distribution on the wall (Re = 1000). The horizontal axis is the angle from the front stagnation point, $\theta' = 180^\circ - \theta$. The velocity u_r is made dimensionless by U_∞.

Figures 5(a) and 5(b) show the time traces of the dissipation rate, ε, and the drag coefficient, C_D:

$$C_D = \frac{F_D}{\frac{1}{2}\rho U_\infty^2 D L_z}, \tag{38}$$

where $F_D = F_{DP} + F_{DF}$ is the total drag force and $L_z = 1$ is the unit spanwise cylinder length. In both cases, ε and C_D abruptly increase right after the control is turned on at $t/T = 15$ and monotonically decrease after that. As summarized in Table I, the present suboptimal control results in higher reduction rates of drag and dissipation rate than those in the J_1-control case.

Figure 5(c) shows the lift coefficient, defined as

$$C_L = \frac{F_L}{\frac{1}{2}\rho U_\infty^2 D L_z}, \tag{39}$$

where F_L is the lift force. In both cases, oscillations immediately decay and eventually vanish, indicating that the flows become steady.

The mechanism of drag reduction can be explained by modifications of the pressure and the friction on the surface. Figures 6(a) and 6(b) show the distributions of the pressure coefficient, C_p, and the friction coefficient, C_f, defined using the local mean pressure, $\overline{p}_w$, and the local mean friction, $\overline{\tau}_w$, as

$$C_p = \frac{\overline{p}_w - p_\infty}{\frac{1}{2}\rho U_\infty^2} \tag{40}$$

and

$$C_f = \frac{\overline{\tau}_w}{\frac{1}{2}\rho U_\infty^2}. \tag{41}$$

The drag reduction is primarily due to the significant recovery of pressure as compared to the uncontrolled case. As minor effects, the pressure coefficient near the front stagnation point is slightly decreased due to the nonzero velocity by the suction. A significant difference between the J_1 control and the present control is also observed near $\theta' = 80^\circ$, although this difference contributes little to the pressure drag. As shown in Fig. 6(b), in the controlled cases, the friction coefficient in the front half is

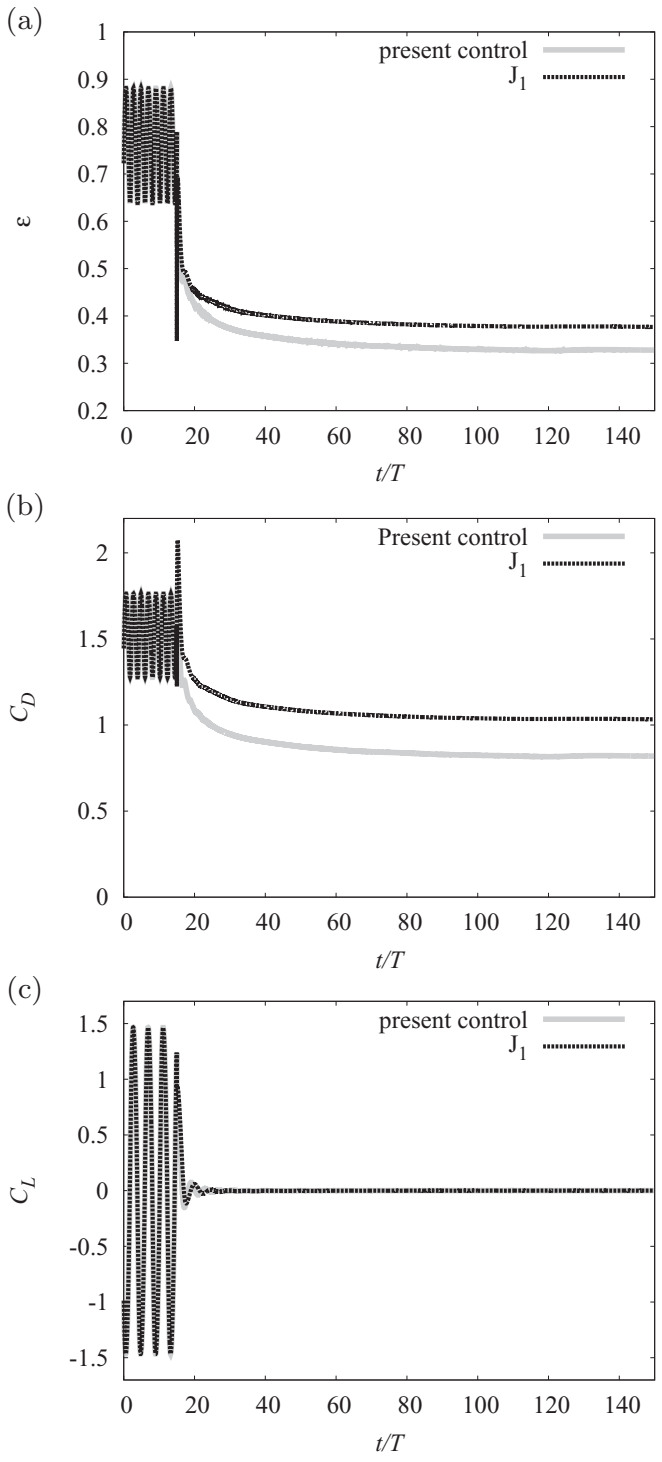

FIG. 5. Time traces (Re = 1000): (a) energy dissipation, ε; (b) drag coefficient, C_D; (c) lift coefficient, C_L. The dissipation rate ε is made dimensionless by ρ, U_∞, and D.

increased due to the suction. The amount of increase is less in the present suboptimal control case due to a weaker suction.

The instantaneous energy dissipation rate fields are shown in Fig. 7. In the uncontrolled case, a large energy dissipation takes place in the shear layer involving vortex shedding. In the controlled cases, in contrast, the dissipation due to vortex shedding has disappeared. Although the dissipation fields in two controlled cases are indistinguishable at a glance, the boundary layer in the present suboptimal control case is found to be slightly thicker than that in the J_1-control case due to the weaker suction.

B. Predetermined control

The results above imply that a similar control effect may also be achieved by a predetermined (i.e., open-loop) control, which does not require any sensors. In this subsection we briefly present some of the results of a predetermined control. In the present predetermined control, the control input is given by the steady profile obtained in the suboptimal control (Fig. 4).

In Fig. 8 the time traces of the energy dissipation rate and the drag coefficient are compared with those of the suboptimal control case. Although a small difference is observed immediately after the control is turned on, the variations in both cases are quite similar in the later period. An excellent agreement can also be observed in the mean surface pressure coefficient, as shown in Fig. 9.

From these results, we can conclude that a predetermined control minimizing the energy dissipation rate is possible, and it has almost the same effects as the suboptimal feedback control.

C. Energy efficiency

In contrast to the ideal actuation power, W_{id}, given by Eq. (14), the maximum possible actuation power can be expressed as [5]

$$W_a = \int_0^{2\pi} \left(\frac{1}{2}|\phi^3| + |p\phi| + \frac{2}{\mathrm{Re}}\frac{1}{R}\phi^2 \right) R\, d\theta. \tag{42}$$

Denoting the drag in the uncontrolled case by F_{D0}, the ideal energy efficiency is given by

$$\gamma_{id} = \frac{U_\infty(\overline{F_{D0}} - \overline{F_D})}{\overline{W_{id}}}, \tag{43}$$

where the overbar denotes the time average. Similarly, the lowest possible energy efficiency is given by

$$\gamma_a = \frac{U_\infty(\overline{F_{D0}} - \overline{F_D})}{\overline{W_a}}. \tag{44}$$

Note that the actual energy efficiency takes a value between γ_{id} and γ_a [5]. The mean drag coefficient, $\overline{C_D}$, the mean drag force, $\overline{F_D} = \overline{C_D}/2$ (since F_D is made dimensionless by U_∞ and D), the mean dissipation, $\overline{\varepsilon}$, the actuation powers, $\overline{W_{id}}$, $\overline{W_a}$, and the energy efficiencies, γ_{id}, γ_a, are tabulated in Table I.

The ideal power, $\overline{W_{id}}$, takes negative values in all cases, indicating that the control is achieved without an external power if the actuators themselves are equipped with a function that recycles the power received from the flow. This is what is meant by the negative values of ideal power and efficiency. From the viewpoint of net energy saving, one profits if the energy efficiency is greater than unity. The lowest energy efficiency, η_a, is below unity in the J_1-control case. In contrast, it is greater than unity in the present suboptimal and predetermined controls.

TABLE I. Drag, dissipation, input power, and energy efficiencies (Re = 1000, two-dimensional flow).

	$\overline{C_D}$	$\overline{F_D}$	$\overline{\varepsilon}$	$\overline{W_{id}}$	$\overline{W_a}$	$\overline{\eta_{id}}$	$\overline{\eta_a}$
No control	1.545	0.773	0.773				
J_1 control	1.037	0.518	0.378	−0.140	0.324	−1.807	0.784
Present suboptimal control ($\Delta t_c/T = 0.75$)	0.864	0.432	0.328	−0.104	0.202	−3.326	1.680
Present predetermined control	0.864	0.432	0.328	−0.105	0.203	−3.249	1.676
Localized predetermined control (Sec. VE)	0.940	0.470	0.367	−0.103	0.122	−2.945	2.479

D. Dependency on the control amplitude

So far the control amplitude has been fixed at $\phi_{\max} = 0.4$ (made dimensionless by U_∞). Here we examine different values of control amplitude, $\phi_{\max} = 0.1$, 0.2, 0.3, and 0.5, to investigate its dependency on the control effect.

Figure 10(a) shows the total energy dissipation in the optimum cases (with respect to the parameter $\Delta t_c/T$) at different control amplitudes. The results of the J_1 control are also plotted for comparison. Compared to the J_1 control, the energy dissipation is reduced more with the present control at larger control amplitudes ($\phi_{\max} \geqslant 0.3$), while it takes similar values at smaller amplitudes ($\phi_{\max} \leqslant 0.2$). This tendency can be explained by Eqs. (11)–(15). When the control amplitude is smaller, the contribution of $F_{D\phi}$ and W_{id} to the present cost function become smaller. Moreover, since the contribution of the friction F_{DF} is small at this Reynolds number, the contribution of the pressure drag F_{DP} is dominant. Therefore, the present cost function approaches the cost function J_1 at smaller control amplitudes.

The lowest possible energy efficiencies η_a at different control amplitudes are plotted in Fig. 10(b). The tendency of the energy efficiency is similar to that of the energy dissipation. When the control amplitude is small, η_a in the present control

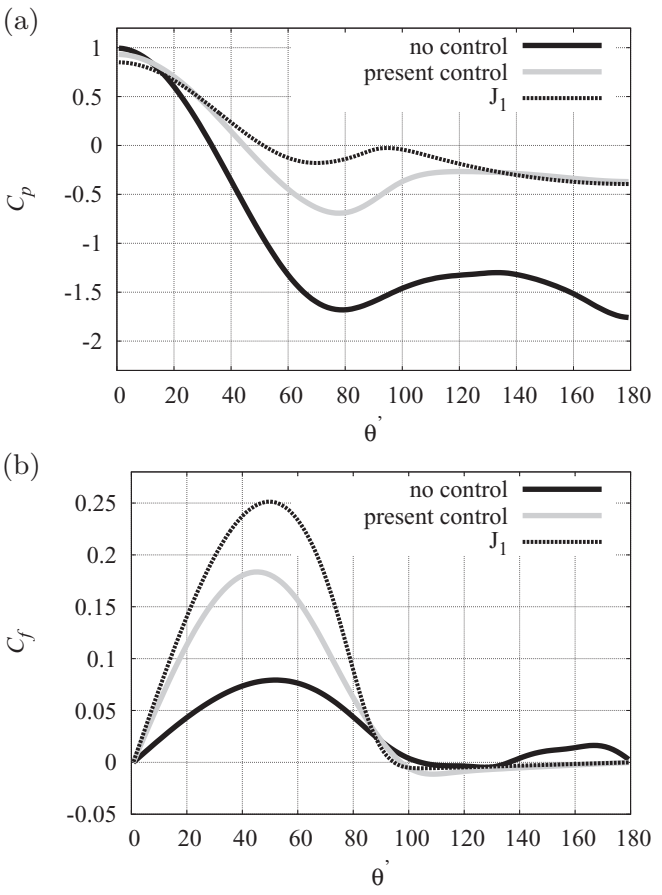

FIG. 6. Pressure and friction coefficients on the cylinder surface (Re = 1000): (a) pressure coefficient, C_p; (b) friction coefficient, C_f. The horizontal axis is the angle from the front stagnation point, $\theta' = 180^\circ - \theta$.

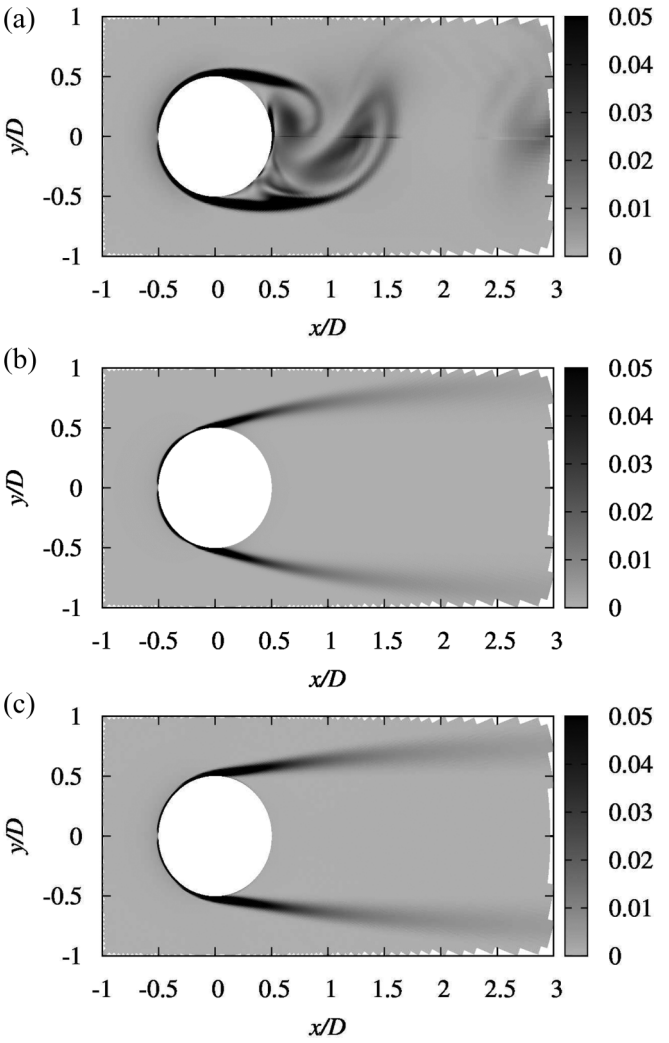

FIG. 7. Instantaneous energy dissipation field (Re = 1000): (a) no control; (b) J_1 control; (c) present suboptimal control ($\Delta t_c/T = 0.75$). The local dissipation rate is made dimensionless by ρ, U_∞, and D.

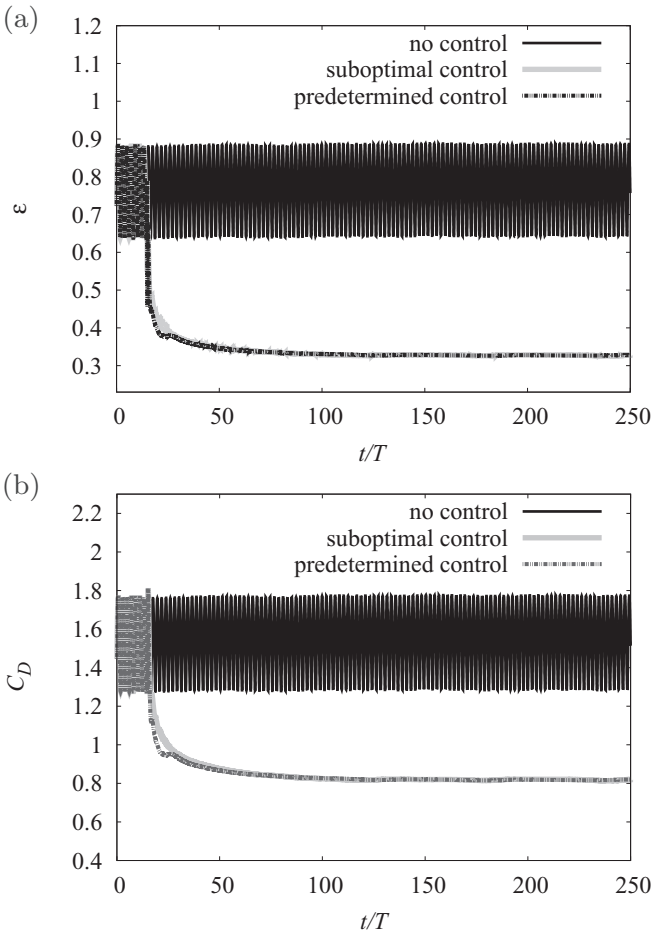

FIG. 8. Time traces in the predetermined control case (Re = 1000): (a) energy dissipation, ε; (b) drag coefficient, C_D. $\theta' = 180^\circ - \theta$. The dissipation rate ε is made dimensionless by ρ, U_∞, and D.

takes similar values to those in the J_1 control, while η_a in the present control takes higher values at $\phi_{\max} \geqslant 0.3$. Note that the present control guarantees the energy profit ($\eta_a > 1$) at any

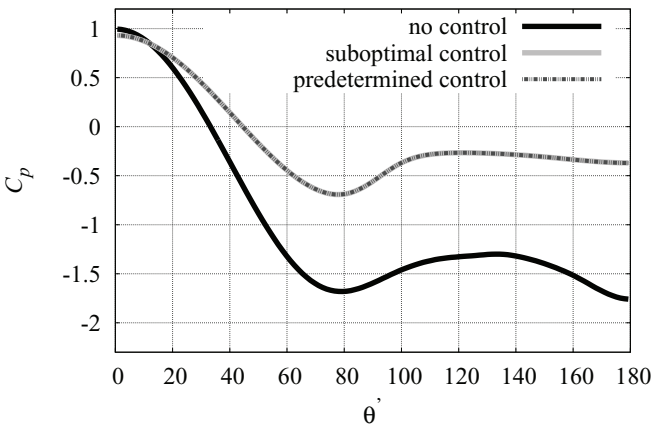

FIG. 9. Surface pressure coefficient in the predetermined control case (Re = 1000). The horizontal axis is the angle from the front stagnation point, $\theta' = 180^\circ - \theta$.

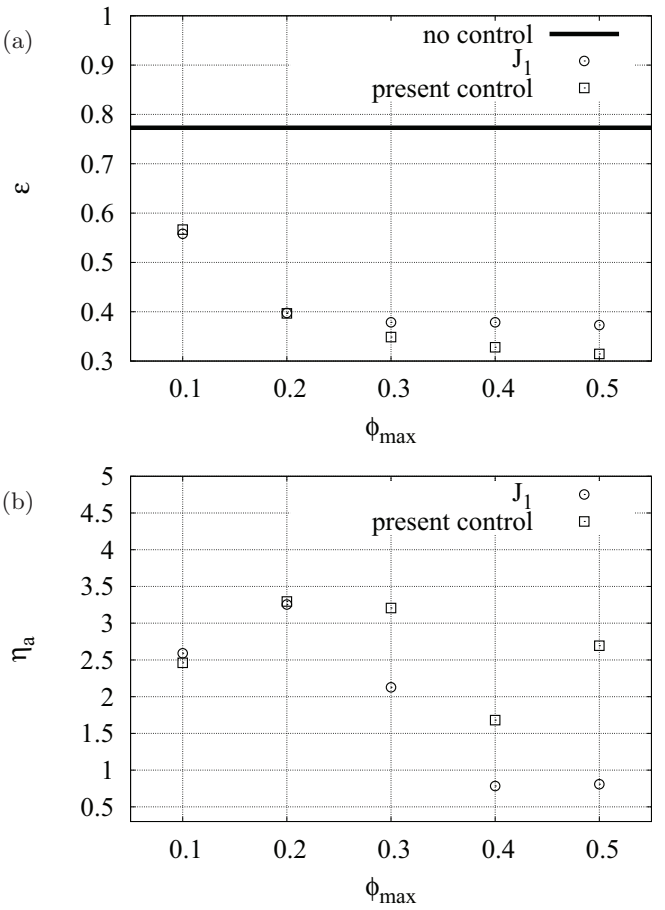

FIG. 10. Dependency on the control amplitude $\phi_{\max}$ (Re = 1000): (a) energy dissipation $\overline{\varepsilon}$; (b) lowest possible efficiency η_a. The dissipation rate ε is made dimensionless by ρ, U_∞, and D.

control amplitudes in contrast to the J_1 control at $\phi_{\max} = 0.4$ and 0.5.

E. Localized control

While the control was so far applied continuously on the entire cylinder surface, it is considered difficult to implement it in practice. Toward its practical implementation, we consider here a predetermined control with localized actuation.

The localized control profiles are obtained by fitting polynomials to the control input distribution shown in Fig. 11. The polynomial and its range are determined so that the zero net flux condition is satisfied. Here, as an example, a quadratic function, $\phi(\theta') = 0.4 - \theta'^2$, and a cubic function, $\phi(\theta') = -0.278 + 0.5252|\theta' - \pi|^3$, are chosen in the range of $-0.2\pi \leqslant \theta' \leqslant 0.2\pi$ and $0.77\pi \leqslant \theta' \leqslant 1.23\pi$, respectively.

The instantaneous energy dissipation field is shown in Fig. 12. Even in the case where the actuation is applied locally (about 40% of the entire surface), the vortex shedding is found to disappear similarly to the continuous cases (Fig. 7).

The computed mean quantities are shown on the last line of Table I. The drag of the present localized control is found to be lower than those in the uncontrolled case and the J_1 control. Although the resultant energy dissipation of the localized control is higher than that of the present suboptimal

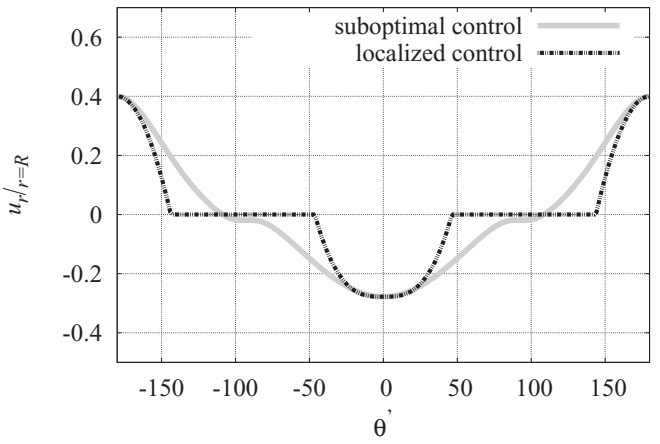

FIG. 11. Velocity distribution on the wall (localized control, Re = 1000). The horizontal axis is the angle from the front stagnation point, i.e., $\theta' = 180^\circ - \theta$. The velocity u_r is made dimensionless by U_∞.

and predetermined controls, the local control shows still better performance than the J_1 control on the entire surface. It is also found that the lowest energy efficiency $\overline{\eta_a}$ is higher than the present suboptimal and predetermined controls due to its lower actuation power $\overline{W_a}$. From the above, it can be said that the present localized control works as efficiently as the continuous case.

F. Control effect in three-dimensional flow

Finally, we examine the control effect in a three-dimensional flow around a circular cylinder at Re = 1000. To avoid the huge computational cost, we adopt the predetermined control input obtained in the two-dimensional flow. For comparison, we also perform the J_1 control.

Figure 13 shows the instantaneous energy dissipation fields. Similarly to the two-dimensional cases, both the J_1 and the present predetermined controls achieve complete suppression of vortex shedding, and the wake region of the J_1 control is found to be slightly wider in lateral direction than that of the present predetermined control.

The control effects are summarized in Table II. The present predetermined control results in a lower energy dissipation than the J_1 control. The drag $\overline{F_D}$ and the maximum possible

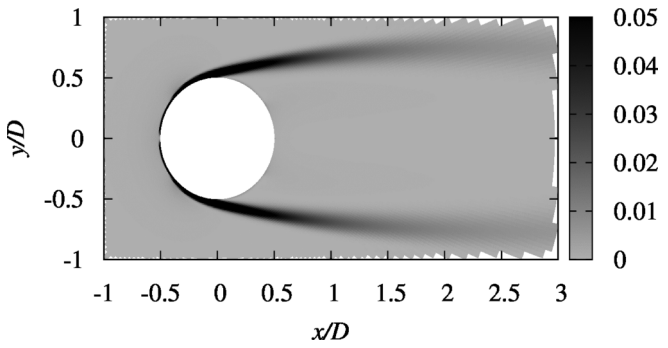

FIG. 12. Instantaneous energy dissipation field (localized control, Re = 1000). The local dissipation rate is made dimensionless by ρ, U_∞, and D.

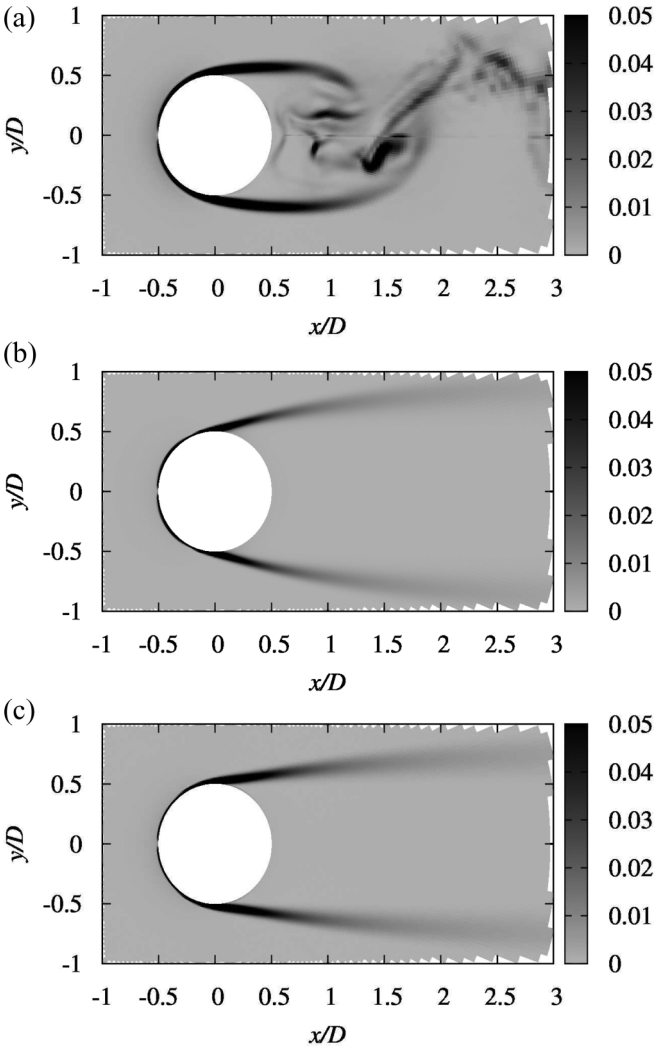

FIG. 13. Instantaneous energy dissipation field (Re = 1000, three-dimensional): (a) no control; (b) J_1 control; (c) present predetermined control. The local dissipation rate is made dimensionless by ρ, U_∞, and D.

power $\overline{W_a}$ of the present predetermined control are found to be lower than those of the J_1 control, which leads to a greater value of $\overline{\eta_a}$. Note that $\overline{\eta_a}$ of the present predetermined control is greater than unity, while the J_1 control is less than unity; it indicates that the total power can be saved by the present predetermined control, while not by the J_1 control.

VI. SUMMARY

A blowing and suction control of a flow around a circular cylinder has been conducted aiming at minimization of the energy dissipation.

To minimize the energy dissipation rate in an infinitely large volume, we have derived the proper cost function, which is expressed by the quantities on the surface. The cost function is then minimized by using the suboptimal control procedure of Min and Choi [6].

Performance of the present suboptimal control has been assessed using two-dimensional numerical simulations at

TABLE II. Drag, dissipation, input power, and energy efficiencies in three-dimensional flow (Re = 1000).

	$\overline{C_D}$	$\overline{F_D}$	$\overline{\varepsilon}$	$\overline{W_{id}}$	$\overline{W_a}$	$\overline{\eta_{id}}$	$\overline{\eta_a}$
No control	1.141	7.165	7.165				
J_1 control	1.037	6.512	4.748	−1.764	2.456	−0.370	0.266
Present predetermined control	0.820	4.121	3.092	−1.029	1.553	−1.959	1.298

Re = 100 and Re = 1000. A parametric study has been conducted for the arbitrary parameter contained in the suboptimal control law, Δt_c. Although no improvement is obtained at Re = 100, the present suboptimal control shows better performance at Re = 1000 than the suboptimal controls previously proposed. Suction near the front stagnation point and blowing in the rear half are weakened in different manners as compared to those in the suboptimal control targeting at pressure drag reduction.

A steady predetermined control based on the suboptimal control has also been performed. The results show that the energy dissipation and the drag can be reduced similarly to those in the suboptimal control. In terms of the lowest possible efficiency, too, the present suboptimal and predetermined controls are shown to have much higher efficiency than the suboptimal control previously proposed.

The computations at different control amplitudes show that the advantage of the present control becomes clearer at higher control amplitudes, and this is explained by the form of the cost function. A similar control effect is also obtained with a localized control based on the obtained predetermined control. Finally, the present predetermined control is shown to work well in the three-dimensional flow at Re = 1000 too.

ACKNOWLEDGMENTS

The authors are grateful to Drs. Shinnosuke Obi, Keita Ando, Akiko Matsuo, and Hiromitsu Kobayashi (Keio University), and Dr. Yukinori Kametani (KTH) for fruitful discussion. This work was supported through Grant-in-Aid for Scientific Research (C) (No. 25420129) by the Japan Society for the Promotion of Science (JSPS).

[1] J. Kim, Phys. Fluids **15**, 1093 (2003).
[2] N. Kasagi, Y. Suzuki, and K. Fukagata, Annu. Rev. Fluid Mech. **41**, 231 (2009).
[3] M. A. Leschziner, H. Choi, and K.-S. Choi, Phil. Trans. R. Soc. A **369**, 1349 (2011).
[4] J. Kim, Phil. Trans. R. Soc. A **369**, 1396 (2011).
[5] H. Choi, W.-P. Jeon, and J. Kim, Annu. Rev. Fluid Mech. **40**, 113 (2008).
[6] C. Min and H. Choi, J. Fluid Mech. **401**, 123 (1999).
[7] J. Kim and T. R. Bewley, Annu. Rev. Fluid Mech. **39**, 383 (2007).
[8] K. Fukagata, K. Sugiyama, and N. Kasagi, Physica D **238**, 1082 (2009).
[9] H. Lamb, *Hydrodynamics*, 6th ed. (Cambridge University Press, Cambridge, 1932), Art. 343, pp. 614–617.
[10] H. Choi, R. Temam, P. Moin, and J. Kim, J. Fluid Mech. **253**, 509 (1993).
[11] S. Jeon and H. Choi, Int. J. Heat Fluid Flow **31**, 208 (2010).
[12] H. Naito and K. Fukagata, Phys. Fluids **24**, 117102 (2012).
[13] K. Fukagata and N. Kasagi, J. Comput. Phys. **181**, 478 (2002).
[14] P. R. Spalart, R. D. Moser, and M. M. Rogers, J. Comput. Phys. **96**, 297 (1991).
[15] J. K. Dukowicz and A. S. Dvinsky, J. Comput. Phys. **102**, 336 (1992).